 doi:10.20944/preprints202103.0123.v1

Article

Fly ash waste recycling by Pt/TiO_2 incorporation for industrial dyes removal

Maria VISA[1], Mihaela COSNITA[1], Macedon MOLDOVAN[1], Cosmina Andreea MARIN[2], Maria MIHALY[2,3,*]

[1] Transilvania University of Brasov, Research center: Renewable Energy Systems and Recycling, Eroilor 29, 500036 Brasov, Romania
[2] University POLITEHNICA of Bucharest, Research Center for Environmental Protection and Eco-Friendly Technologies (CPMTE), Bucharest, Romania
[3] University POLITEHNICA of Bucharest, Faculty of Applied Chemistry and Materials Science, Inorganic Chemistry, Physical Chemistry and Electrochemistry Department, Polizu 1, RO-011061, Bucharest, Romania
* Correspondence: maria.mihaly@upb.ro

Abstract: New materials are obtained by transforming fly ash wastes into a valuable composite, with tandem adsorption and photodegradation properties. Mild hydrothermal synthesis, from titanium dioxide, Platinum nanoparticles and zeolite materials obtained from a waste, fly ash, as support, was involved in the composite preparation. The Platinum nanoparticles extended the photocatalytic activity of the composite in Visible range (Eg = 2.1 eV). The efficiency of tandem adsorption and photocatalytic activity of the new composite were evaluated to 80.70% for Bemacid Blau and 93.89% for Bemacid Rot, after 360 min, the irradiation time, with H_2O_2 addition.

Keywords: fly ash waste; platinum nanoparticles; industrial dyes; adsorption; photodegradation

1. Introduction

Increasingly intense and diverse industrial activity raises major issues of environ-mental protection. It is, on the one hand, the discharge of pollutants into the environment, either accidentally or due to the inefficiency of removal methods. For example, the dyes are dangerous pollutants and must be removed immediately [1]. Most of these are carcinogenic, harmful and reduce the light penetration in aqueous systems causing the photosynthesis process, so being harmful to aquatic live and of course to human health.

On the other hand, it is about industrial waste dumps. Among them are the flying ashes (FA) from power plants. Depending upon the source and composition of the coal being burned, the components of fly ash vary considerably, but all fly ash includes substantial amounts of silicon dioxide (SiO_2) (both amorphous and crystalline), aluminum oxide (Al_2O_3), iron oxide (Fe_2O_3) and calcium oxide (CaO). Their physical, chemical, and min-eralogical properties suggest the opportunities for their use and disposal.

A contextual approach, namely, the use of fly ash waste to develop effective solutions in the removal of industrial dyes, can help to reduce their negative effect on the environ-ment.

The industrial dyes have in their chemical structure one, two or more aromatic rings with chromophore groups, as the azo group (–N=N–), which gives them high stability, and are therefore difficult to degrade [2,3].There are several processes investigated: co-agulation [4], adsorption [2], aerobic or anaerobic biosorption [5,6] and advanced chem-ical oxidation or photochemical degradation [7-10]. Of these, photochemical degradation is one of the most effective.

Photochemical degradation uses different semiconductor oxides (TiO_2, WO_3, SnO_2) with photocatalytic activity. Titanium dioxide (TiO_2) is the most widely used photo-catalyst because of its properties, such as non-toxic, low cost, strong oxidation power and high chemical stability. One of the shortcomings of this procedure is the difficulty to

Preprints (www.preprints.org) | NOT PEER-REVIEWED | Posted: 3 March 2021 doi:10.20944/preprints202103.0123.v1

separate the liquid and the solid photocatalyst after removing the pollutants. For this reason, the researchers have been explored many solid substrate [11-13] to immobilize WO_3, TiO_2 [14]. Thus, FA, by its composition (especially SiO_2, Al_2O_3 and unburned carbon) could be a suitable support material to be optimized as an adsorbent with potential photo-catalytic properties (depending on the burned coal source and composition, small quantities of TiO_2, MnO_2 can be found in FA). The limited efficiency of photocatalytic ac-tivity comes from the high rate of electron-hole recombination into semiconductors par-ticles, TiO_2, in this case. Various heterogeneous catalysts have been extensively studied to enhance the efficiency of organic pollutants degradation, such as: doping metal ions into the TiO_2 lattice [15], noble metals (Pt, Pd, Au, Ag) addition on TiO_2 surface [16-20], de-posited on an inert matrix such as fly ash [21] or incorporation of photoactive TiO_2 in an aluminosilicate inorganic polymer [22].

Based on these considerations, an excellent research opportunity is created, and the main objective of this study is to use fly ash waste as a source for photoadsorbant ma-te-rials production. This paper aims to demonstrate, by a detailed investigation, a tech-nically feasible way to combine non-energy raw materials from different sources (Ro-manian fly ash resulted by burning of harder, older anthracite and bituminous coal, in this case) and quality (F type - the sum of SiO_2, Al_2O_3 and Fe_2O_3 is over 70%) with TiO_2 semiconductor and Pt nanoparticles (PtNP). The influence of H_2O_2 on the degradation efficiency of industrial dyes is also evaluated.

Finally, a hybrid procedure, based on adsorption, photo oxidation and chemical oxidation, is proposed to efficient degrade some industrial dyes, Bemacid Rot (BR) and Bemacid Blau (BB).

2. Materials and Methods

2.1. Materials

Fly ash (FA) used in this study was collected from Heating Plant CET Brasov, Ro-mania. This FA is a cheap material, a poly-oxide compound with a high percentage of SiO_2 (53.32%), Al_2O_3 (22.05%) and of Fe_2O_3 (8.97%). According to the ASTM standard C-618-2a [23], this fly ash is of F type (the sum of SiO_2, Al_2O_3 and Fe_2O_3 is over 70%). In addition to these major oxides, others were identified (TiO_2 - 1.07%, Mn_2O_3 - 0.08%) in the FA composition, which act as photocatalysts for organic pollutants photodegradation. Besides, the unburned carbon (1.58%) can act as an efficient adsorbent of dyes and heavy metals.

The TiO_2 content was increased by FA mixing with Degussa P25 (anatase: rutile ratio = 3:1), with 55 m^2/g BET surface, particle size around 30 nm and 97% purity.

Stable dispersion of cysteamine modified - platinum nanoparticles (Pt-Cys NP) were synthesized using polyoxyethylene-4-lauryl ether (Brij 30), n-heptane and cysteamine monoclorhidrate (CS) provided by Sigma-Aldrich. Also ultrapure Millipore water was used for the preparation of the samples. All the other reagents were analytical grade and were used without further purification.

The synthetic wastewaters were prepared by using bi-distilled water and the in-dustrial dyes: Bemacid Rot N-TF (BR) with azo group (-N=N-) and auxochrome groups (–OH, $–NH_2$, $–SO_3Na$) and Bemacid Blau N-TF (BB) with auxochrome groups ($–SO_3Na$, $–NH_2$, –NH–) and anthraquinone chromophore group (Figure 1), from Bezema AG, Switzerland. BB and BR are used in dyeing of cotton and they are highly resistant to biodegradation.

Preprints (www.preprints.org) | NOT PEER-REVIEWED | Posted: 3 March 2021 doi:10.20944/preprints202103.0123.v1

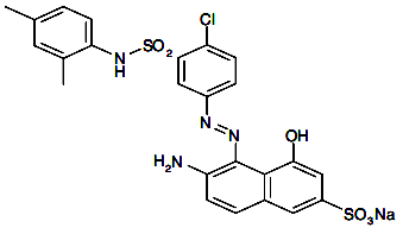

Bemacid Rot N-TF (BR)

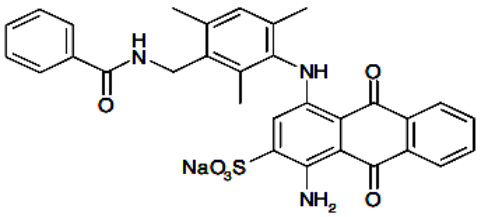

Bemacid Blau N-TF (BB)

Figure1. Chemical structures of the dyes.

2.2. Materials preparation procedures

2.2.1. Preparation of Pt-Cys NP

Pt-Cys NP were obtained using microemulsion assisted photoreduction technique (MAPR), a procedure like one previously published by authors to synthesize AuNPs [24]. This consists in the reduction of platinum precursor under UVC light irradiation (λ = 254 nm) in water-in-oil (W/O) microemulsion template (82.5 % n-heptane, 15% Brij 30, 2.5% $HAuCl_4$ 1g·L^{-1}), in the presence of cysteamine monoclorhidrate ligand (Cys) used as stabilizers, until the colour of the microemulsion changes showing the formation of Pt-Cys NP.

2.2.2. Preparation of photocatalytic adsorbent materials

The preparation method of the new composite material is as follow. First, fly ash particles, with size between 40-100 μm, and NaOH pellets were fused at high temperature, 500°C, during 3h, followed by cooling at room temperature. Then, the material was crushed and mixed with de-ionized water for 1h until a suspension is formed. The en-richment of materials with TiO_2 was done by adding, under stirring (300 rpm), Degussa P25 and kept in an autoclave, at atmospheric pressure and 100°C, for 24h. After this time, the stirring was interrupted, and the suspension has been preserved for 24h at 100°C for nucleation in alkaline environment. The suspension was filtered, rinsed for several times with double distilled water and dried at 105-115°C for 12h.

To increase and extend the photocatalytic activity of the nanocomposite powder, by stopping the recombination of the e- with h+, positive charged platinum nanoparticles (Pt-Cys NP) were added.

The resulted composite, with adsorbent and photocatalytic properties, active in UV and Vis, is denoted FADPt.

2.3. Structure and surface characterization

The crystalline structure and variations in chemical structure of FADPt composite were investigated by using an X-ray Diffractometer (XRD Bruker D8 Discover Diffrac-tometer, Kα1= 1.5406Å, 40kW, 20mA, step size 0.02, scan speed 2 sec/step, 2θ range ranging from 10 to 80°). The surface morphology (roughness and macro-pores size dis-tribution) was studied using Scanning Electron Microscopy (SEM S-3400N-Hitachi, ac-celerating voltage of 20KV) and Atomic Force Microscope (AFM Ntegra Spectra, NT-MDT model BL222RNTE). The images were taken in semi-contact mode with Si-tips (NSG 10, at constant force 0.15N/m. with 10nm tip radius). The size, shape and crystallinity of the samples have been observed by High Resolution Transmission Electron Microscopy performed on a PHILIPS CM 120 ST HR-TEM. Energy Dispersive X-ray (EDX, Thermo Scientific Ultra Dry) was used to outline the surface elemental composition. The XPS spectra were recorded on a Thermo Scientific K-Alpha equipment, fully integrated with an aluminum anode monochromatic source. Survey scans (0-1200eV) were performed to identify constitutive elements. The Fourier-Transform Infrared Spectroscopy was used to identify the new chemical changes. The FT-IR spectra of the new composite

Preprints (www.preprints.org) | NOT PEER-REVIEWED | Posted: 3 March 2021 doi:10.20944/preprints202103.0123.v1

were recorded with Spectrum BX Perkin Elmer BXII 75548, λ= 400–4000 nm. The surface energy was calculated. The reflectance spectrum was taken using a UV-Vis-NIR Spectrometer (Perkin Elmer Lambda 25 UV/Vis) and the data were used to evaluate the optical band gap (Eg) of the samples.

Static contact angle measurements based on the sessile drop method were recorded and analyzed using an OCA-20 Contact Angle –meter (Data Physics Instruments).

Micro-porosity and BET specific surface were measured using an Autosorb-IQ-MP, Quantachrome Instruments.

2.4. Tandem adsorption and photodegradation experiments

The photodegradation experiments were run using a homemade vertical tubular photocatalytic reactor (Figure 2 (a)) with two concentric quartz tubes, which works in con-tinuous flow with suspensions. The radiation source consists of a series of 11 LEDs (LED-tube 600 mm 8 W/865 cool daylight tubes, Philips CorePro, emitting Vis light, 400–700 nm, λmax =5450 nm, G =8 W/m2) and 11 UV tubes (F18W/T8/24/BL368 - UVA lamp, BL368 tubes emit an upgraded highly concentrated radiation with peak around 368 nm, G=18W), interchangeable, positioned around the external surface of the quartz tube (Figure 2 (b)) to prevent scattering and to ensure uniform distribution. The radiance for each experiment is G = 208.7 W/m^2 with the energy consumption of 2.52 KWh. The substrate dose is 0.6 g/L.

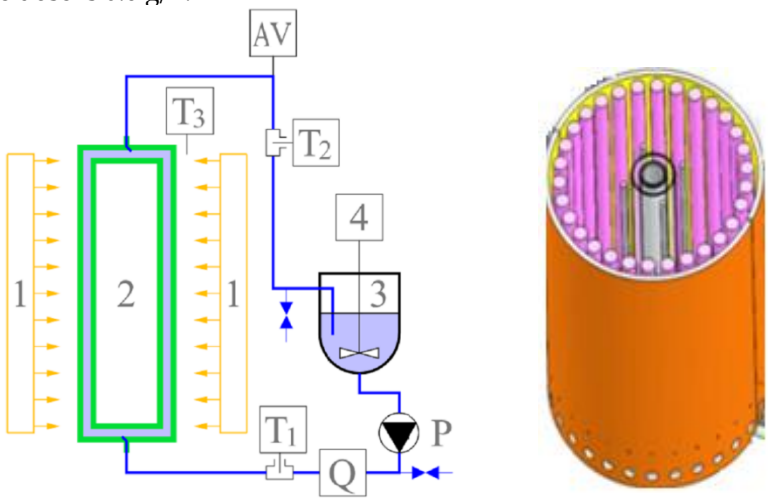

(a) (b)

Figure 2. Functional scheme of the photo-reactor (a) and detail of the cylindrical quartz tube inside of the lighting system (b)

1 - LEDs and UV lamps; 2 - Cylindrical quartz tube; 3 - Storage tank; 4- Electric overhead stirrer; AV- Air vent; P- Hydraulic pump; Q- Flowmeter; T1-Inlet temperature sensor; T2 -Outlet temperature sensor; T3- Ambient air temperature sensor [25].

The synthetic wastewaters solution contains 50 mg/L BR or 50 mg/L BB. Conse-quently, for each experiment, 3 g FADPt and 5 L solution were introduced into the res-ervoir of the reactor, without and with different volumes of H2O2 30% (4, 8 and 12 mL), under continuous recirculation, assured by the peristaltic pump, with 61-65 L/h, for 30 min, in dark, to reach the adsorption –desorption equilibrium before irradiation. Thus, the active species generated by photoirradiation could attack the organic pollutants if these are in the very close proximity of activated sites.

Independent adsorption experiments were done, in continuous flow, at room tem-perature, 23±1°C, without H_2O_2, to quantify the adsorption contribution to the pho-to-degradation efficiency on FADPt. The composite dose and the initial concentrations of pollutants are like that in photocatalysis process. Since the uptake rates of dye onto FADPt are of great importance with regards to potential scale-up and implementation of this system to remove pollutants from water, kinetic studies have been conducted. Aliquots were taken at fixed moments (30…up to 360 min), a time long enough to reach adsorption of the dyes. After filtration (0.45 μm), the pollutant concentrations were

Preprints (www.preprints.org) | NOT PEER-REVIEWED | Posted: 3 March 2021 doi:10.20944/preprints202103.0123.v1

measured and calculated on a calibration curve, at the maximum absorption peaks (for BR (λBR= 501 nm) and for BB (λBB= 629 nm)). The adsorption test was conducted using quartz tube, and dye losses due to adsorption on the walls of the tube and on the filter paper were negligible. The tests were performed in triplicate and the deviations are less than 3%. The removal efficiency of the dyes by adsorption/photodegradation was obtained by relating at Eq. (1).

$$\eta = \frac{C_o - C_t}{C_o} \cdot 100, [\%] \quad (1)$$

where C_o - the initial concentration and C_t the dye`s concentration at moment t.

The adsorption and photodegradation processes were investigated at natural working pH of the suspension (pH = 7.89-8.04).

3. Results and discussion

3.1. Characterization of the composite

3.1.1. Crystalline structure

The diffraction peaks of the hetero-structures (Figure 3 (A)) confirm that in this system, the fussion above 550°C, hydrothermal and ultrasound, were sufficient to obtain a polycrystalline surface, zeolites, TiO_2, platinum-titanium (Pt-TiO_2) and platinum-silicone (Pt-SiO_2). In the diffraction pattern of the FADPt, two additional peaks, corresponding to the crystallographic planes JCPDS 00-001-1194 of Pt at 2θ = 40.03° and 45.55° are detected and has a cubic crystallite cell with 19.59 nm. On the FADPt difractogram, the shape of the peaks appears as overlapping, meaning that this substrate contains semiconductor oxides homogenously dispersed within the composite, which indicates the existence of a high number of contact aluminosilicate (zeolite-NaP1, gomelinite, illite-montmorill onite) with TiO_2. The alkaline hydrothermal treatment also initiated TiO_2 recrystallization process on the micro-sized aluminosilicates, extending the crystallites dimensions. Based on the XRD results, the crystallite sizes were calculated by using the Scherrer equation. The crystallites sizes are influenced by the ratio of the nucleation in alkaline hydrothermal process. It is also to notice that FADPt will contain all three TiO_2 polymorphs: anatase has a tetragonal crystalline cell (JCPDS 00-001-0562) with 13.18 nm crystallite size, rutile has a tetragonal crystalline cell (JCPDS 00-001-1292) with 8.50 nm crystallite size and brookite has orthogonal crystalline cell (JCPDS 00-016-0617) with 8.15 nm crystallite size. The overall crystalline degree of FADPt is estimated at 79.33%, the rest being amorphous phases and after adsorption/photocatalysis of BR the crystalline degree is 79.10% (Figure 3 (B)).

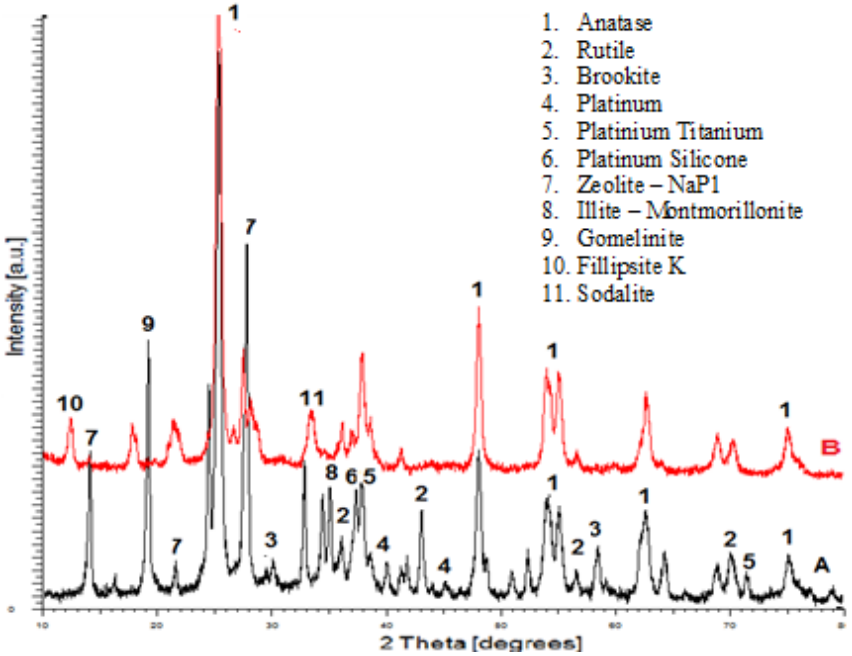

Preprints (www.preprints.org) | NOT PEER-REVIEWED | Posted: 3 March 2021 doi:10.20944/preprints202103.0123.v1

Figure 3. XRD patterns: (A) before adsorption/photocatalysis; (B) after adsorption/photocatalysis.

The composition of the main components in the powder composite is presented in Table 1. Several studies have shown that the materials based on Pt or Au nanoparticles incorporated on composite with TiO2 are much improved charge transfer and thus increase catalyst performance [26].

Table 1. The composition of the FADPt.

Components of FADPt	Anatase	Rutile	Brookite	Pt (Np)	Zeolite NaP1	Other
Composition (%)	43.99	1.81	1.79	0.88	17.14	35.27

3.1.2. Surface morphology

The porosity assays were performed using the adsorption-desorption technique on solid samples. The specific surface area (SBET) and pores distribution were analyzed, and the results are presented in Table 2. Corroborating the data provided by adsorption-desorption isotherms and pores volume, based on the BJH for the analyzed sample, it can be concluded that this is non-porous material with small microporosity areas.

Table 2. Surface characteristics of FA and FADPt.

Sample	S_{BET} (m^2/g)	$V_{Micropores}$ (cm^3/g)	$D_{Average\ pores}$ (nm)	Surface Energy		E_g (eV)
				Polar (mN/m)	Dispersive (mN/m)	
FA	6.14	0.0042	27.2	58.43	5.54	2.45
FADPt	40	0.17	35	88.90	1.42	2.12

The information on the polarity, surface energy and surface wetting behavior are important parameters for substrates used in adsorption/photocatalysis of the pollutants from aqueous solutions. The adsorption of the cations involves electrostatic forces therefore the surface energy of the composite (FADPt) can strongly influence the adsorption process. The contact angle values (θ) of the composite (FADPt) measured using water as wetting liquid was low (5-10°) proving a good surface wettability. The surface energy (σ) (polar and dispersive) was obtained from test liquids with different polarities: glycerol (with polar component of the surface $\sigma_S^p = 41.50$ =41.50 mN/m) and ethylene glycol (with polar component of the surface $\sigma_S^p = 19.00$ mN/m). According to Owens and Wendt, the FADPt composite surface energy has a predominant polar nature, which indicates the hydrophilic surface and wettability, making them a suitable composite with dual applications (adsorbent and photocatalysts) in simultaneous removal of dyes from wastewater [27]. The polar component ($\sigma_S^p = 41.50$= 88.90 mN/m) of the surface energy with $\sigma_S^p > \sigma_S^d$ (Table 2), is the result of increased crystalline to 79.33% of the composite. The FADPt composite, with a large polar component and a high crystallinity, can adsorb better the dyes molecules.

The AFM images (Figure 4) show, in addition to uniform grains, that the composite also contains the aggregates with various shapes and sizes (Table 3). These shapes can also be seen on the surface of the substrates loaded with adsorbent dyes.

Preprints (www.preprints.org) | NOT PEER-REVIEWED | Posted: 3 March 2021 doi:10.20944/preprints202103.0123.v1

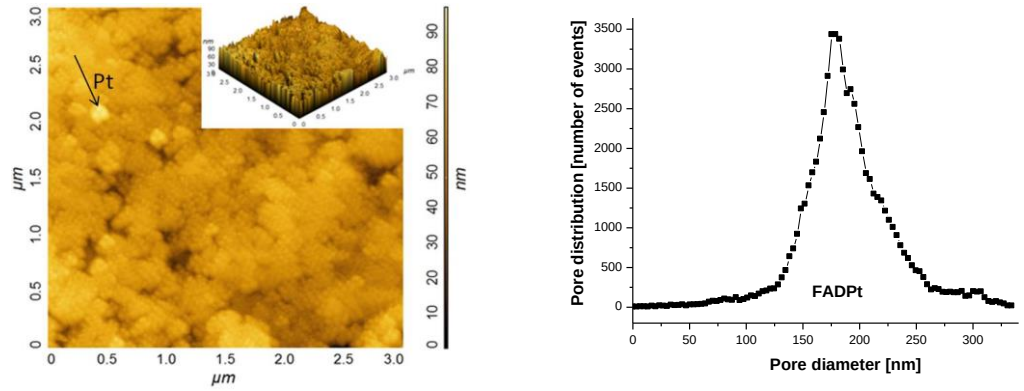

(a) Average Roughness: 49.436nm (a`) Pore histogram for FADPt

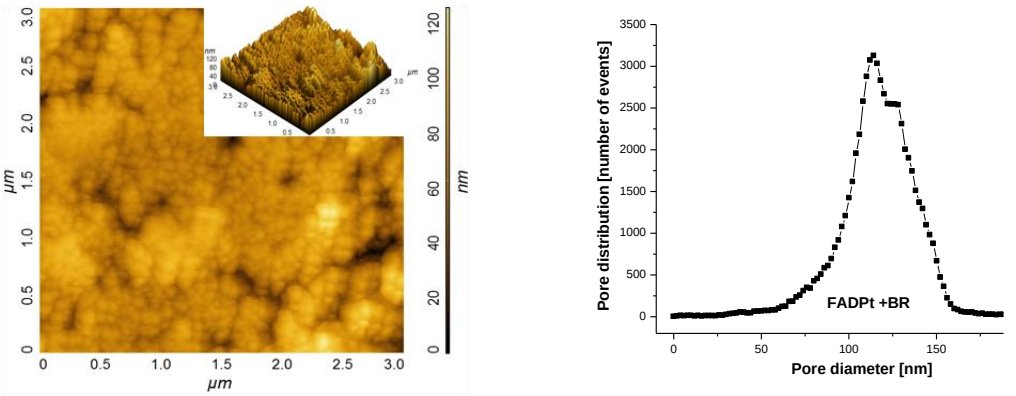

(b) Average Roughness: 69.788nm (b`) Pore histogram for FADPt +BR

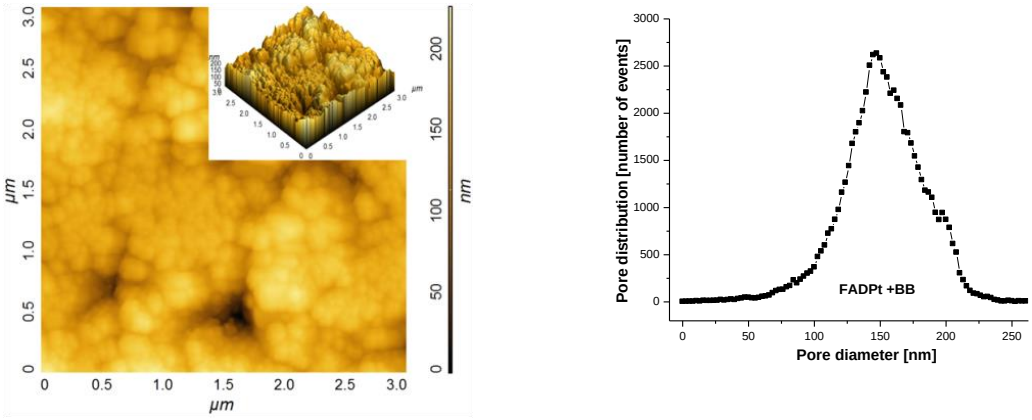

(c) Average Roughness: 156.066nm (c`) Pore histogram for FADPt+BB

Figure 4. AFM topography, average roughness and pore distribution before and after adsorption/photocatalysis for: a) FADPt; b) FADPt loaded with BR; c) FADPt loaded with BB.

Table 3. The parameters of grains analyzed based on AFM images.

Sample	Area (μm^2)	Volume ($\mu m^2 nm$)
FADPt/grain	0.049	3.269
FADPt loades with BR/grain	0.872	6.946

Preprints (www.preprints.org) | NOT PEER-REVIEWED | Posted: 3 March 2021 doi:10.20944/preprints202103.0123.v1

FADPt loades with BB/grain	0.916	18.621

The particles sizes after adsorption/photocatalysis increased (Table 3) and higher roughness was recorded from 49.436 nm (Figure 4 (a)) to 69.788 nm (Figure 4 (b)) and 156.01 nm (Figure 4 (c)), respectively. Adsorption of the BB dye with a large molecule developed a surface with high roughness compared with adsorption of BR dye, the molecule with four aromatic rings and an azo group.

The pore size distribution was estimated on AFM data using the method described by Otero et al. [28]. The results show that FADPt pores (Figure 4 (a)) are narrower (< 200 nm) than that of the washed fly ash (FA) 0.4 -1.1 μm [21]. Responsible for these changes can also be the incorporation of the quite uniform of TiO_2 Degussa P25 powder, in the large pores of the FA, forming aggregation with anatase, rutile or brookite [29]. The size of individual grains is close to 2.69 - 3.07 μm and of the grains from agglomerates is above 24.00 μm (Figure 5 (b)).

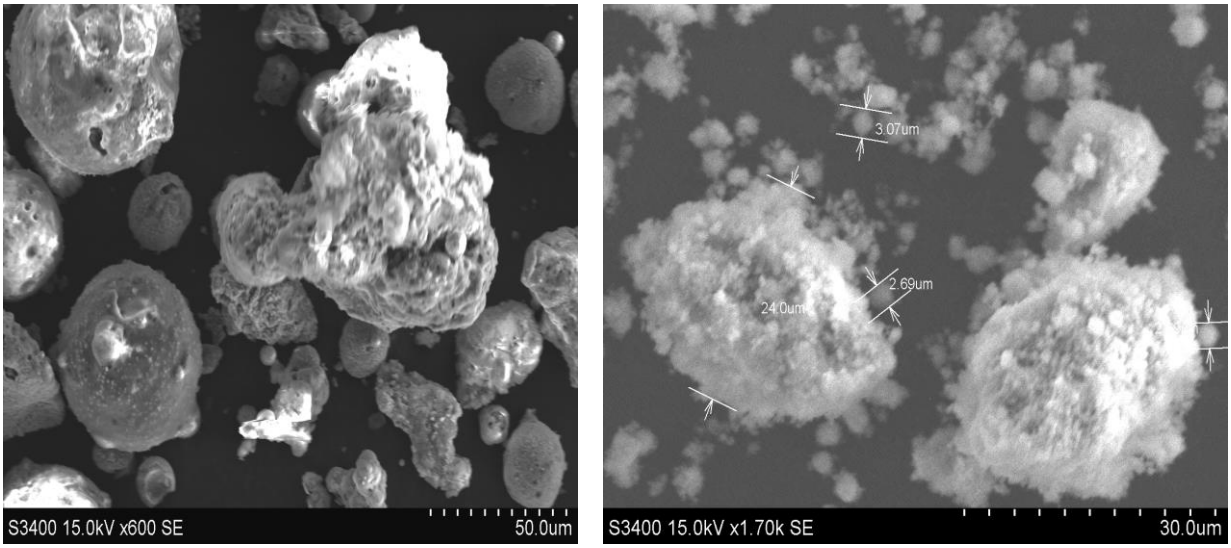

(a) (b)

Figure 5. SEM images of (a) FAw; (b) FADPt.

The AFM, SEM and EDX patterns show an ordered and homogeneous distribution of the TiO_2 nanoparticles onto FADPt composite. The active sites suggest a favourable adsorption and photodegradation processes of the dyes. This assumption is supported by other studies on the modification of the FA surface during the hydrothermal or even simple alkali treatment and/ or the presence of other oxides like (e.g. TiO_2) [21]. Adsorption is likely to start inside the larger micro-pores, therefore the distribution curves are shifted to lower values of the diameters, with a predictable increase in the roughness (Figure 4 (c)).

The heterostructure of the composite was characterized by TEM microscopy and is shown in Figure 6. Pt nanoparticules are associated in mezoagregate with zeolite and TiO_2. TEM microscopy images recorded for Pt-CS NP show that they have a spherical shape and dimensions between 10 -15 nm.

Preprints (www.preprints.org) | NOT PEER-REVIEWED | Posted: 3 March 2021 doi:10.20944/preprints202103.0123.v1

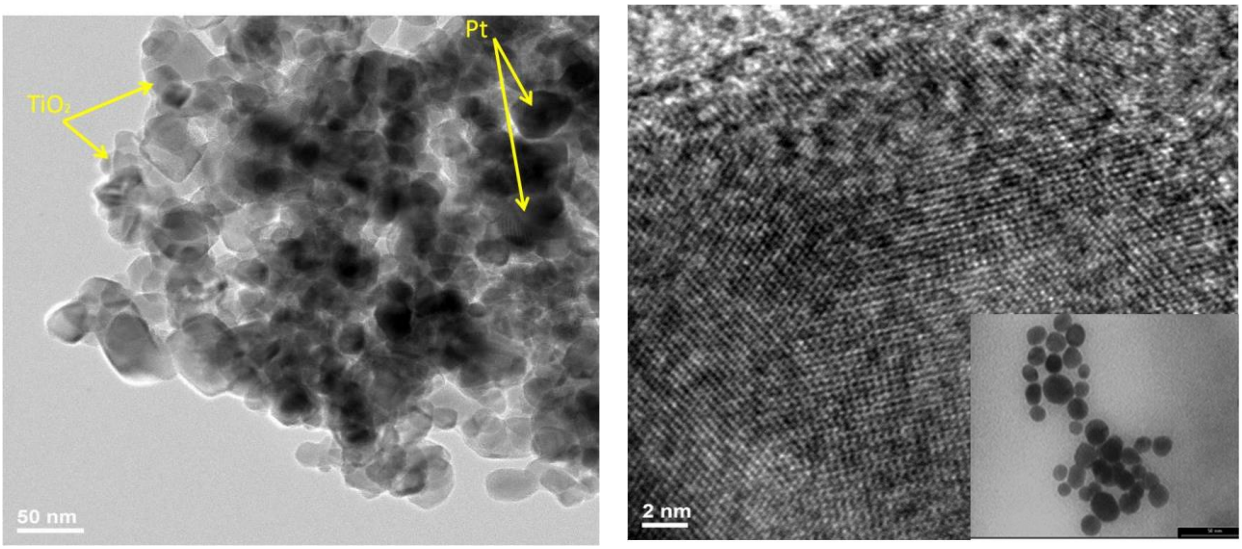

(a) (b)

Figure 6. High magnification TEM image showing platinum nanoparticles aggregate on the TiO_2.

HR-TEM images reveal {100} and {111}d-spacings, similarly reported by others for shaped Pt nanoparticles [30,31]. The images presented in Figure 6 show the characteristic sheets of the layered TiO_2, zeolite, confirming that, although disordered, the solids maintain the intrinsic organization of the layered TiO_2 and zeolite. The EDX spectrum and mapping images were done and the results are included in Figure 7 and Table 4, respectively. The EDX mapping (Figure 7) suggests a homogeneous distribution of Pt nanoparticles located between the anatase, rutile and aluminosilicates.

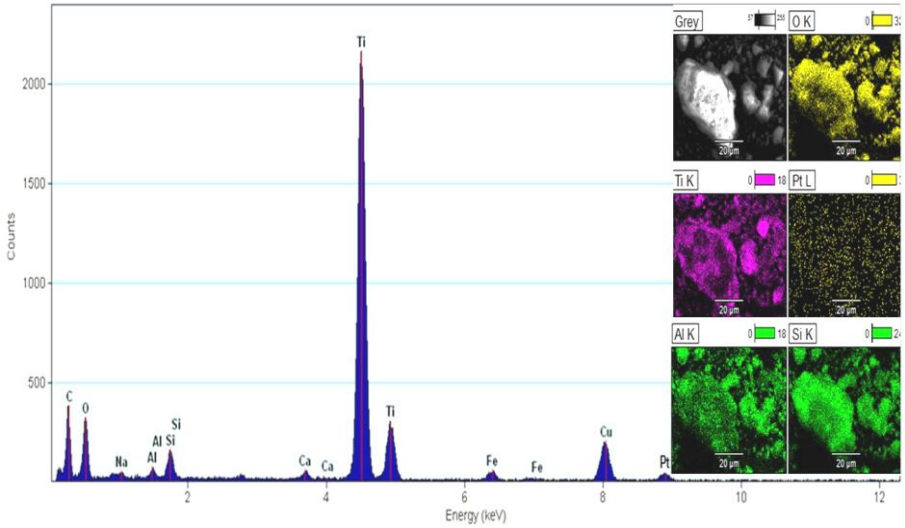

Figure 7. EDX spectrum and mapping images of FADPt.

Table 4. Surface composition, in element Wt % and atomic %, of the FADPt surface before and after loaded with BR and BB dyes.

Element Line	Element Wt.before (%)	Atom before (%)	Element Wt.(%) Substrate loaded with BR	Atom (%) Substrate loaded withBR	Element Wt.(%) Substrate loaded with BB	Atom (%) Substrate loaded with BB
C K	1.94	4.84	60.44	62.90	2.15	5.61
N K	0	0	18.18	17.54	11.38	16.39

Preprints (www.preprints.org) | NOT PEER-REVIEWED | Posted: 3 March 2021 doi:10.20944/preprints202103.0123.v1

O K	18.89	35.38	14.2	12.1	47.07	58.38
Na K	3.01	3.92	0.35	0.23	2.42	2.12
Mg K	0.99	1.32	0.08	0.05	0.11	0.09
Al K	2.61	2.9	0.77	0.38	4.18	2.13
Si K	12.81	13.62	0.85	4.41	4.92	3.54
S K	0	0	0.01	0.3	0.11	0.07
Ca K	22.9	17.13	0.32	0.41	1.58	0.8
Ti K	32.36	20.2	4.75	1.47	25.98	10.86
Pt M	4.49	0.69	0.05	0.21	0.1	0.01
Total	100.00	100.00	100.00	100.00	100.00	100.00

The nitrogen and sulphur content data prove that the BR and BB dyes were adsorbed onto the substrate or were photodegraded. Also, the organic or inorganic carbon on the surface of the composite increased after adsorption/ photodegradation, suggesting accommodation or decomposition of the dyes in organic compounds with smaller molecules.

3.1.3. UV-Vis diffuse reflectance spectra

By coupling two, three semiconductors or semiconductors with noble metals with suitable electronic band (SiO_2, TiO_2, WO_3, Pt, Au, Ag), the photocatalytic activity under UV or Vis irradiation could be improved. The composite FADPt (Eg = 2.1 eV) is more active in visible light and it can involve other compounds from the substrate at working pH = 7.89. More rigorously, the band gap of the semiconductor, in this case a mixture of semiconductors and Pt, is obtained from optical measurements based on the reflectance spectra. The results are presented in Table 2.

3.1.4. X-ray photoelectron spectroscopy

XPS was carried out and the binding energies of the main peaks (Ti 2p, O1s, Al 2p, Si 2p Pt 4d and Pt 4f) are listed in Table 5. The peak fixed at 459.1 eV corresponds to Ti4+ oxidation state in all three TiO2 polymorphs [18] and confirms the buildup of TiO2 nanoparticles on the zeolites (O1s, Al 2p, Si 2p). The O1s peak centered at 531eV is assigned to oxygen from oxides with Si, Al, Na, Ca atoms or to oxygen from hydroxyl groups on surface. The signal of Pt 4f is very small due to the low Pt NP content in the sample (Figure 8). The atomic percentages of the elements calculated by XPS were found smaller than EDX results (Figure 7).

Table 5. Binding energy and the atomic % of FADPt.

Element	Binding Energy (eV)	Atomic %
O1s	531	52.07
Ti2p	459.1	13.24
Na1s	1072.77	9.79
Si2p	103.18	8.58
C1s	286.03	8.64
Ca2p	347.91	1.81

Preprints (www.preprints.org) | NOT PEER-REVIEWED | Posted: 3 March 2021 doi:10.20944/preprints202103.0123.v1

Al2p	75.11	4.01
Pt4d	315.08	1.45
Pt4f	75.08	0.40

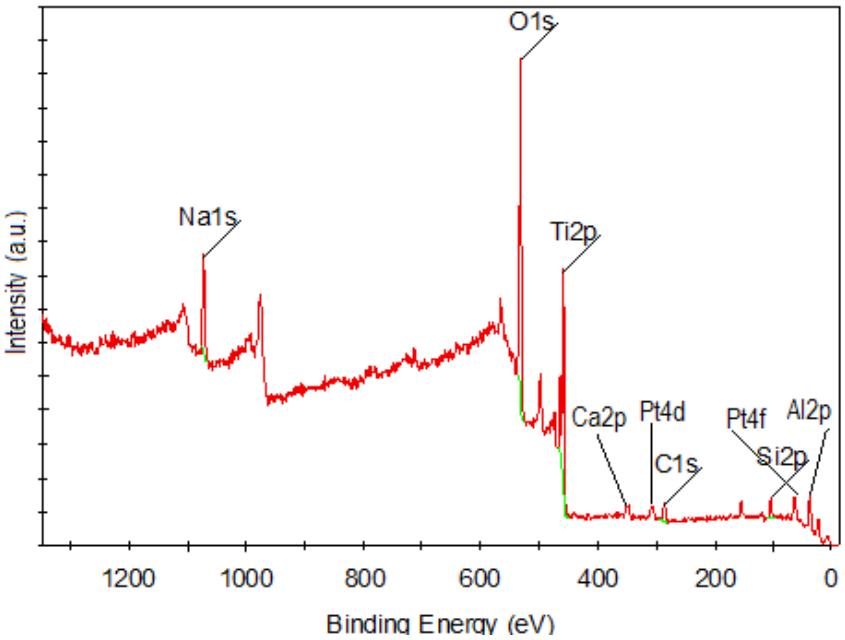

Figure 8. XPS spectrum of FADPt composite.

3.1.5. FT-IR analysis

The FT-IR spectra (Figure 9) of FADPt composite before and after photodegradation/adsorption of dyes BB and BR were performed to investigate the vibration frequency changes of the functional groups, which represent the number of adsorption bonds that identify the type of chemical bonds, indicating the complex nature of the adsorbent (Table 6).

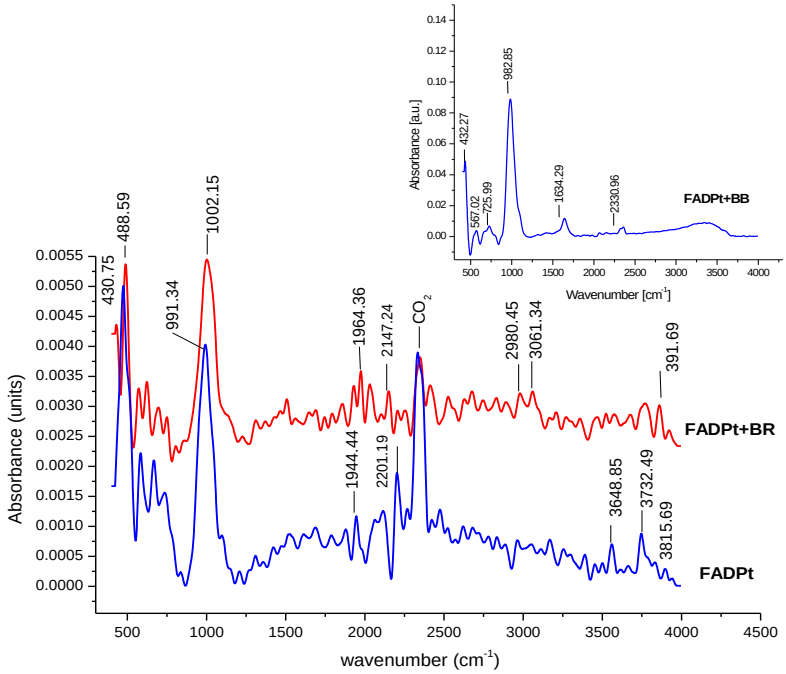

Figure 9. FTIR spectrum of: FADPt, FADPt loaded with BR, FADPt loaded with BB.

The peaks located at 1615 and 1678 cm-1 are indexed for O–H (bonding water molecules).The sharp and intens peaks were recorded at 1002, 990, 982, 997 cm-1, which are

Preprints (www.preprints.org) | NOT PEER-REVIEWED | Posted: 3 March 2021 doi:10.20944/preprints202103.0123.v1

attributed to the asymmetric stretch of Ti – O – Si; Si – Al – O; Al – O; Si – O. The broad band around 425, 447 cm-1 is characteristic to O – Ti – O bridging vibration from rutile. The linear carbonyl Pt^{3+}, Pto–CO, identified at 2176 cm-1 in FADPt and inreveals a shift in the case of FADPt loaded with BR was recorded at to higher frequency (2246 cm-1), suggesting that the Pt nanoparticles interacted with BR dye. Also, a weak band of Pt – (CO) – Pt was registered at 1918 and 1873 cm-1 for the initial material and in FADPt loaded with BR, respectively. All these changes prove the positive effect of Pt nanoparticles on photodegradation processes of the industrial dyes.

Table 6. Characteristics of IR bands associated with FADPt, FADPt with BB loaded and FADPt with BR loaded [32, 33].

Characteristics groups	FADPt [cm-1]	FADPt +BB [cm-1]	FADPt+BR [cm-1]
Si – OH intens	3815	-	3931
Si – (OH)Al hydroxyl groups stretching	3730	-	3755
OH groups bridging hydroxyls in zeolite cages to the same Al – OH – Si	3648	-	3661; 3509
Linear carbonyl Pt^{4+}, Pt^{0}-CO,	2176	-	2246;2184;
$[Pt_3CO)_6]^{2-}n$	2195		2111
Pt/Al_2O_3 –(2093 cm^{-1});	2093		
CO adsorbed on Pt atoms	2069	-	2054
Pt^{2+}-CO: 2155, 2141 cm^{-1}	2155		
Weak bands Pt – (CO) - Pt	1918		1873
Water molecules	1615	1642	1678
Si – Al – O; Al – O asymmetric stretch	990	982	997
Ti – O - Si	1002	992	971
O-Ti-O from rutile	425	-	447
Ti – O – Ti bridging vibration	811	730	788,740
Si – O bond of the zeolite structure	689	662	684
HO-Pt-OH stretch vibration	577	561	582

3.2. Tandem adsorption and photodegradation on FADPt

3.2.1. Dyes adsorption on FADPt

The results of the adsorption process are presented at pH = 7.89 (Figure 10 (a)). The efficiency of the experiments run under the radiance of 208.7 W/m2 (Figure 10 (b, c)) and shows an increased efficiency when H2O2 was added.

Preprints (www.preprints.org) | NOT PEER-REVIEWED | Posted: 3 March 2021 doi:10.20944/preprints202103.0123.v1

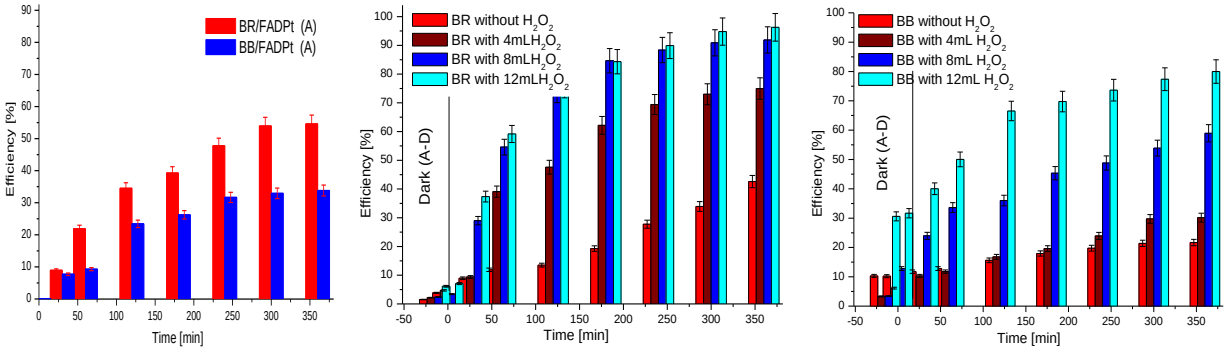

Figure 10. The efficiency of BB and BR dyes removal: (a) by adsorption; (b, c) by photocatalysis.

The adsorption efficiency (53.59% BR and 33.81% BB) depends on the composite characteristics (charge of the surface, morphology, porosity, distribution of the active sites) and the chromophore group of the dye. Both dyes have large molecules and different chromophore groups, anthraquinone in BB dye and azo in BR, groups which have different behavior in contact with active sites on the substrate. During the adsorption process the dye could diffuse onto adsorbent, in micropores and /or could develop weak physical bonds between functional groups (-NH_2, -NH-, -OH, -SO_3Na) and the active sites disposed on TiO_2, on FADPt aggregates, respectively [34].

3.2.2. The combined adsorption and photocatalysis processes

The composite, containing anatase (43.99%), rutile and brookite, is activated by irradiations with an energy higher than the band gap value Eg= 2.1 eV, corresponding to λ =399.9 nm. Under irradiation, the electron-hole pairs are photo-generated on anatase surface, Eq. (2). The oxidative holes $(h+)_{VB}$ can react with H_2O to form active species OH·or will react with hydroxyd ions on the surface (Si - OH) or can directly react with the dyes molecules producing degradation product, Eqs. (3 - 5) [35]. The dye molecules (R-H) will be degradate by the hydroxyl radicals to organic intermediates, smaller organic molecules or inorganic compounds, such as CO_2, H_2O or to other, Eq.(6). The organic intermediates is possible to be more discolored with one aromatic ring, sometimes very difficult to degrade [34,36].

$$2\ TiO_2 + h\nu \rightarrow TiO_2(h+)_{VB} + TiO_2(e-)_{CB} \quad (2)$$

$$TiO_2(h+)_{VB} + H2O_{(ads)} \rightarrow HO\cdot + H+ + TiO_2 \quad (3)$$

$$TiO_2(h+)_{VB} + HO- \rightarrow HO\cdot + TiO_2 \quad (4)$$

$$TiO_2(h+)_{VB} + R\text{-}H \rightarrow \text{Oxidation product} \quad (5)$$

$$R\text{-}H + HO \rightarrow \text{Degradation product} \quad (6)$$

The high charge recombination rate and the wide band gap (rutile - 3.0 eV and anatase 3.2 eV) impose a fundamental restriction on the overall photocatalytic efficiency of TiO_2. By combining TiO_2 with noble metals nanoparticles, such as Pt [17,37], Au [18], Ag [12] and Pd [19], Schottky barriers [38] could be formed, which drive photogenerated electrons from $TiO_2(e-)_{CB}$ to the noble metal (Pt), decreasing the recombination speed of e- with h+ and thus an enhanced photocatalytic activity is obtained, Eq. (7) (Figure 11).

$$Pt^{4+} + TiO2(e-)_{CB} \rightarrow Pt^{3+} + TiO_2 \quad (7)$$

Preprints (www.preprints.org) | NOT PEER-REVIEWED | Posted: 3 March 2021 doi:10.20944/preprints202103.0123.v1

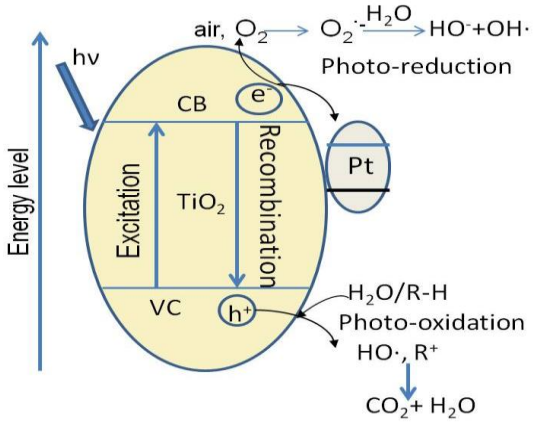

Figure 11. Schematic diagram of photocatalytic mechanism.

3.2.3. The effect of concentration of the H_2O_2 on the photocatalytic process

Photocatalysis is enhanced by a larger amount of hydroxyl radicals, because they are very powerful oxidized, with Eox=2.8V. One way to increase the rate of them is addition of hydrogen peroxide under UV radiations, Eq. (8):

$$H_2O_2 + h\nu \rightarrow 2HO\cdot \quad (8)$$

The optimal parameters for degradation of textile dyes (anionic dyes) are: concentration of dye, H_2O_2 concentrations and working pH. According to some authors, the optimal pH is between 3 - 9 [39,40]. A lot of researchers have investigated the effect of H_2O_2 dosage on the decolourisation of dyes [39]. The degradation efficiency of the dyes increases with addition of H_2O_2 to a certain value, due to the increase in the hydroxyl radical concentration, Eq. (8). The excess of H_2O_2 probably promote the reaction of hydroxyl radicals with H_2O_2 molecules leading to formation of hydroperoxyl radicals (Eq. (9)), these can also react with HO·, reducing the amount of HO,·and thus, decreasing the efficiency of dyes degradation, Eq. (10).

$$HO\cdot + H_2O_2 \rightarrow H_2O + HO_2\cdot \quad (9)$$
$$HO_2\cdot + HO\cdot \rightarrow H_2O + O_2 \quad (10)$$

Based on these studies, the optimum volume of the H_2O_2 30%, which have to added at 5 L BR solution with 3 g substrate, followed by 360 min of irradiation, is 8mL (Table 7). The percentage of 91.88% recorded for BR removal confirms the positive effect of H_2O_2 and reactivity of the BR molecule in photodegradation process. On the other hand, adding 12 mL H_2O_2 at 5 L BB solution, in the same working conditions, leads to an increase in the efficiency of BB dye removal. The molecule of BB is more complex and the maximum efficiency in this case is 79.99%.

Table 7. The influence of oxygen peroxide volume on dye degradation.

Preprints (www.preprints.org) | NOT PEER-REVIEWED | Posted: 3 March 2021 doi:10.20944/preprints202103.0123.v1

	BR - Removal (%)					BB - Removal (%)				
	$V_{H2O2\ (30\%)(mL)}$					$V_{H2O2\ (30\%)(mL)}$				
Time (min)	4	8	12	8-4	12-8	4	8	12	8-4	12-8
120	47.59	73.76	74.50	26.16	0.74	16.80	36.01	66.54	19.21	30.53
180	62.14	84.65	84.33	22.51	-0.32	19.63	45.32	69.77	25.69	24.44
240	69.43	88.39	89.92	18.96	1.53	23.94	48.80	73.65	24.85	24.85
300	72.98	90.89	93.89	17.91	3.00	29.74	53.87	77.37	24.13	23.49
360	74.96	91.88	94.04	16.92	2.15	30.16	58.94	79.99	28.77	21.05

The photodegradation process of dyes with H_2O_2 also depends on their structure (Table 7), but most important is the working pH. In alkaline conditions, the hydrogen peroxide is possible to decomposition to water and oxygen and the production of hydroxyl radicals will be decrease [39], Eq. (11).

$$H_2O_2 \rightarrow H_2O + O_2 \quad (11)$$

The optimum working pH is close to neutral, in this case pH = 7.89.

In the same conditions of irradiation, the BB dye is less degradated in all experiments. The degradation mechanisms are very different, the azo group, with labile π-bonds, is the first target for·HO·, in the case of BR (azo-dye). The sulfonic groups will also react to further produce phenol or other aromatic compounds [35,36], and the amino-groups will eventually form ammonia [37]. In BB dye, the HO· radicals attack the -NH- positions and sulfonic groups leading to a broad range of intermediates derived from the anthraquinone nuclei [34,40,41].

3.3. Kinetics modeling of the adsorption processes

The kinetics models are fitted to the experimental data by the nonlinear regression analysis, according to the pseudo-second order kinetics, given by the equation Eq. (12) [42]:

$$\frac{t}{q_t} = \frac{1}{k_2 q_e^2} + \frac{t}{q_e} \quad (12)$$

where: k_2 is the rate constant for the pseudo-second order adsorption ($g \cdot mg^{-1}min^{-1}$), qt and qe are the amount of adsorbed dyes ($mg \cdot g^{-1}$) at time t (min) and equilibrium.

The linearization proved that the pseudo-second kinetic order well describes the adsorption mechanism for both dyes (Table 8). These results outline again the importance of adsorption as a preliminary step in photocatalysis.

Table 8. Kinetic parameters of the dyes removal in adsorption processes.

Pollutant	Pseudo-second order

Preprints (www.preprints.org) | NOT PEER-REVIEWED | Posted: 3 March 2021 doi:10.20944/preprints202103.0123.v1

(dye)	k_2 (g mg^{-1}min^{-1})	q_e (mg/g)	R^2
BR (A)	2.532	8.024	0.849
BB (A)	4.385	5.204	0.929

3.4. Kinetics modeling of the photocatalysis processes

The kinetics data were modelled using a first kinetics derived from the Langmuir –Hinshelwood model, Eq.(13) [43]:

$$\ln C/Co = - k_{obs}\, t \quad (13)$$

where: c_o and c are initial dye concentration and the concentration at the moment t and k_{obs} is the overall observed pseudo first-order degradation rate constant.

The photodegradation results of the dyes, in working conditions, without and with oxygen peroxide (Figure 12), show that the mechanism follows the pseudo-first order model.

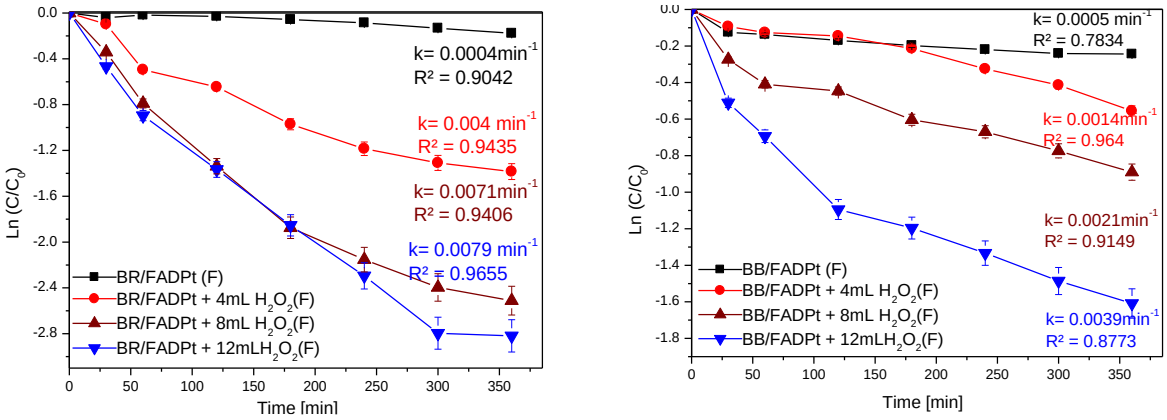

(a) (b)

Figure 12. Photocatalysis of dyes (a) BR; (b) BB.

The BR photodegradation proved also to be faster (k = 0.0079 min-1) as compared to BB (k = 0.0039min-1), thus allowing a more significant amount of oxidizing species to be involved. In the working conditions, pH = 7.89, the oxygen production from H_2O_2 is employed, which afterwards can contribute to decreasing recombination. H_2O_2 was used as an electron scavenger accelerated decolorization and degradation of the BR and BB dyes.

4. Conclusions

Fly ash wastes were efficient recycle to obtain an effective photocatalytic composite by adding nanosized Degussa P25 and positive charged platinum nanoparticles (Pt-Cys NP). The mild hydrothermal process allows obtaining a material with specific surface ten times larger than the initial fly ash.

The FADPt material was tested in tandem adsorption and photocatalysis experiments for removing two industrial dyes, Bemacid Red (azo-dye) and Bemacid Blau (antraquinone-dye). The pseudo-second order kinetic is the model that governs the adsorption process of removing pollutants from complex systems. The addition of H_2O_2 in the working conditions improves the process efficiency up to 96.04% after 360 min. The rate constant of the pseudo first-order process increases from 0.0004 min^{-1}, when the degradation process developed without H_2O_2, to 0.0079 min^{-1}, with H_2O_2.

Author Contributions: Conceptualization, M.V. and M.Mihaly; methodology, M.V. and M.Mihaly; validation, M.V. and M.Mihaly; investigation, M.C., M.Moldovan and C.A.M.; writing—original draft preparation, M.C., M.Moldovan and C.A.M.; writing—review and editing, M.V. and M.Mihaly; visualization, M.V.; supervision, M.V. and M.Mihaly; project administration, M.V. All authors have read and agreed to the published version of the manuscript.

Funding: This research received no external funding.

Institutional Review Board Statement: Not applicable.

Informed Consent Statement: Not applicable.

Acknowledgments: This research was supported by a grant of the Romanian National Authority for Scientific Research, ANCS – UEFISCDI, project PN-II-PT-PCCA-2013-4-0726.

Conflicts of Interest: The authors declare no conflict of interest.

References

1. Safavi, A.; Momeni, S. Highly efficient degradation of azo dyes by palladium/ hydroxiapatite/Fe_3O_4 nanocatalyst. *J. Hazard. Mater.* **2012**, *201-202*, 125-131, https://doi.org/10.1016/j.jhazmat.2011.11.048.
2. Visa, M.; Pricop, F.; Duta, A. Sustainable treatment of wastewaters resulted in textile dyeing industry. *J. Clean Techn. Environ. Policy.* **2012**, *13*, 855-861, https://doi.org/10.1007/s10098-011-0362-4.
3. Malakootian, M.; Almasi, A.; Hossaini, H. Pb and Co removal from paint industries effluents using wood ash. *Environ. Scien. and Techn.* **2008**, *5*, 217-222, https://doi.org/10.1007/BF03326015.
4. Patel, H.; Vashi, R.T. Treatment of textile wastewater by adsorption and coagulation. *E.J. Chemistry.* **2010**, *7*, 1468-1476, https://doi.org/10.1155/2010/987620.
5. Çınar, Ö.; Yaşar, S.; Kertmen, M.; Demiröz, K.; Kitis, M. Effect of cycle time on biodegradation of azo dye in sequencing batch reactor. *Process Saf. Environ.* **2008**, *86*, 455-460, https://doi.org/10.1016/j.psep.2008.03.001.
6. Shaw, C.B.; Carliell, C.M.; Wheatley, A.D. Anaerobic/aerobic treatment of coloured textile effluents using sequencing batch reactors. *Water Res.* **2002**, *36*, 1193-2001, https://doi.org/10.1016/S0043-1354(01)00392-X.
7. Tantak, N.P.; Chaudhari, S. Degradation of azo dyes sequential treatment. *J. Hazard. Mater. B.* **2006**, *136*, 698-705, https://doi.org/10.1016/j.jhazmat.2005.12.049.
8. Jing, G.; Luan, M.; Chen, T. Progress of catalytic wet air oxidation technology. *Arabian J. of Chemistry.* **2016**, *9*, S1208–S1213. https://doi.org/10.1016/j.arabjc.2012.01.001.
9. Visa, M.; Duta, A. Methyl-orange and cadmium simultaneous removal using fly ash and photo-Fenton systems. *J. Hazard. Mater.* **2013**, *244–245*, 773–779, https://doi.org/10.1016/j.jhazmat.2012.11.013.
10. Azizi, A.; Alavi Moghaddam, M.R.; Maknoon, R.; Kowsari, E. Innovative combined technique for high concentration of azo dye AR18 wastewater treatment using modified SBR and enhanced Fenton process as post treatment. *Process Saf. Environ.* **2015**, *95*, 255-264, https://doi.org/10.1016/j.psep.2015.03.012.
11. Sun, P.; Xue, R.; Zhang, W.; Zada, I.; Liu, Q.; Gu, J.; Su, H.; Zhang, Z.; Zhang, J.; Zhang, D. Photocatalyst of organic pollutants decomposition: TiO_2/glass fiber cloth composites. *Catal. Today.* **2016**, *274*, 2-7, https://doi.org/10.1016/j.cattod.2016.04.036.
12. Zang, Q.; Zheng, D.D.; Xu, L.S.; Chang, C.T. Photocatalytic conversion of terephthalic acid preparation wastewater to hydrogen by graphene-modified TiO_2. *Catal. Today.* **2016**, *274*, 8-14, https://doi.org/10.1016/j.cattod.2016.02.010.
13. Legrand, A.; Moissette, A.; Hureau, M.; Casale, S.; Massiani, P.; Vezin, H.; Mamede, A.S.; Batonneau-Gener, I. Electron transfers in a TiO_2-containing MOR zeolite: synthesis of the nanoassemblies and application using a probe chromophore molecule. *Phys. Chem. Chem. Phys.* **2014**, *26*, 13145-13155, https://doi.org/10.1039/C4CP01543F.
14. Andronic, L.; Cazan, C.; Enesca, A.; Visa, M. TiO_2–active carbon composites for wastewater photocatalysis. *J. Sol-Gel Sci. Technol.* **2014**, *71*, 396-405, https://doi.org/10.1007/s10971-014-3393-6.
15. Andronic, L.; Hristache, B.; Enesca, A.; Visa, M.; Duta, A. Studies on titanium oxide catalyst doped with heavy metals (cadmium, copper and nickel). *Environ. Engin. Manag. J.* **2009**, *8*, 747-751, http://omicron.ch.tuiasi.ro/EEMJ/pdfs/vol8/no4/29_Andronic.pdf.
16. Chen, Y.H.; Chen, L.L.; Shang, N.C. Photocatalytic degradation of dimethyl phthalate in an aqueous solution with Pt-doped TiO_2-coated magnetic PMMA microspheres. *J. Hazard. Mater.* **2009**, *172*, 20–29, https://doi.org/10.1016/j.jhazmat.2009.06.122.
17. Mohapatra, S.K.; Kondamudi, N.; Banerjee, S.; Misra, M. Functionalization of self-organized TiO_2 nanotubes with Pd nanoparticles for photocatalytic decomposition of dyes under solar light illumination. *Langmuir.* **2008**, *24*, 11276–11281, https://doi.org/10.1021/la801253f.
18. Vaiano, V.; Iervolino, G.; Sannino, D.; Murcia, J.J.; Hidalgo, M.C.; Ciambelli, P.; Navio, J.A. Photocatalytic removal of patent blue V dye on Au-TiO_2 and Pt-TiO_2 catalysts. *Appl. Catal. B-Environ.* **2016**, *188*, 134-146, https://doi.org/10.1016/j.apcatb.2016.02.001.

19. Visa, M.; Andronic, L.; Enesca, A. Behavior of the new composites obtained from fly ash and titanium dioxide in removing of the pollutants from wastewater. *J. Appl. Surf. Sci.* **2016**, *388*, 359-36912, https://doi.org/10.1016/j.apsusc.2015.12.154.
20. Wang, H.; Niu, J.; Long, X.; He, Y. Sonophotocatalytic degradation of methyl orange by nano-sized Ag/TiO_2 particles in aqueous solutions. *Ultrason. Sonochem J.* 2008, *15*, 386-392, https://doi.org/10.1016/j.ultsonch.2007.09.011.
21. Visa, M.; Duta, A. TiO_2/fly ash novel substrate for simultaneous removal of heavy metals and surfactants. *Chem. Engin. J.* **2013**, *223*, 860-868, https://doi.org/10.1016/j.cej.2013.03.062.
22. Gasca-Tirado, J.R.; Manzano-Ramirez, A.; Villaseñor-Mora, C.; Muñiz-Villarreal, M.S.; Zaldivar-Cadena, A.A.; Rubio-Ávalos, J.C.; Borráse, V.A.; Mendoza, R.N. Incorporation of photoactive TiO_2 in an aluminosilicate inorganic polymer by ion-exchange. *Microp. Mesopor. Mat.* **2012**, *153*, 282–287, https://doi.org/10.1016/j.micromeso.2011.11.026.
23. Ramme, B.W.; Tharaniyil, M.P. *Coal Combustion Products Utilization Handbook*, 2nd ed.; Publisher: Manufactured in the U.S. of America, America, 2004; pp. 15–18.
24. Mihaly, M.; Fleancu, M.C.; Olteanu, N.L.; Bojin, D.; Meghea, A.; Enachescu, M. Synthesis of gold nanoparticles by microemulsion assisted photoreduction method. *C. R. Chim.* **2012**, *15*, 1012-1021, https://doi.org/10.1016/j.crci.2012.09.013.
25. Visa, M.; Duta, A.; Visa, I.; Moldovan, M.; Neagoe, M. Continuous flow tubular reactor for simultaneous photocatalysis and suspension adsorption processes. Patent application, a 201600536, **2016**.
26. Zhang, N.; Liu, S.; Xu, Y.J. Recent progress on metal core@semiconductor shell nano-composites as a promising type of photocatalyst. *Nanoscale.* **2012**, *4*, 2227–2238, https://doi.org/10.1039/C2NR00009A.
27. Owens, D.K.; Wendt, R.C. Estimation of the surface free energy of polymers. *J. Appl. Polym. Sci.* **1969**, *13*, 1741–1747, https://doi.org/10.1002/app.1969.070130815.
28. Otero, J.A.; Mazarrasa, O.; Villasante, J.; Silva, V.; Pradanos, P.; Calvo, J.I.; Hernandez, A. Three independent ways to obtain information on pore size distributions of nanofiltration membranes. *J. Membr. Sci.* **2008**, *309*, 17-27, https://doi.org/10.1016/j.memsci.2007.09.065.
29. Ökte, A.N.; Karamanis, D.; Tuncel, D. Dual functionality of TiO_2–flyash nanocomposites: water vapor adsorption and photocatalysis. Catal. Today. **2014**, *230*, 205–213, https://doi.org/10.1016/j.cattod.2014.01.031.
30. Zhang, B.; Wang, D.; Hou, Y.; Yang, S.; Yang, X.H.; Zhong, J.H.; Liu, J.; Wang, H.F.; Hu, P.; Zhao, H.J.; Yang, H.G. Facet-dependent catalytic activity of platinum nanocrystals for triiodide reduction in dye-sensitized solar cells, *Sci. Rep*. **2013**, *3*, 1836, https://doi.org/10.1038/srep01836.
31. Jason, M.A.; Morris, W.H.; Lukehart, C.M. Synthesis of shaped Pt nanoparticles using common anions or small molecules as shape-directing agents: observation of a strong halide or pseudo-halide effect. *J. Mater. Chem. A.* **2015**, *3*, 2012-2018, https://doi.org/10.1039/C4TA05952B.
32. Devi, L.G.; Kumar, S.G. Exploring the critical dependence of adsorption of various dyes on the degradation rate using Ln^{3+}-TiO_2 surface under UV/solar light. Appl. Surf. Sci. **2012**, *261*, 137– 146, https://doi.org/10.1016/j.apsusc.2012.07.121.
33. Visa, M.; Isac, L.; Duta, A. Fly ash adsorbents for multi-cation wastewater treatment. *Appl. Surf. Sci.* **2012**, *17*, 6345-6352, https://doi.org/10.1016/j.apsusc.2012.03.035.
34. Duta, A.; Visa, M. Simultaneous removal of two industrial dyes by adsorption and photocatalysis on a fly-ash-TiO_2 composite. *Photochem. Photobiol. A-Chem.* **2015**, *306*, 21-30, https://doi.org/10.1016/j.jphotochem.2015.03.007.
35. Stem, N.; De Souza, M.L.; Araujo de Faria, D.L.; Dos Santos Filho, S.G. Formation of Ti(III) and Ti(IV) states in Ti_3O_5 nano- and microfibers obtained from hydrothermal annealing of C-doped TiO_2 on Si. *Thin Solid Films*. **2014**, *558*, 67-74, https://doi.org/10.1016/j.tsf.2014.02.077.
36. Gözmen, B.; Kayan, B.; Gizir, A.M.; Hesenov, A. Oxidative degradations of reactive blue 4 dye by different advanced oxidation methods. *J. Hazard. Mater.* **2009**, *168*, 129–136, https://doi.org/10.1016/j.jhazmat.2009.02.011.
37. Ohtani, B.; Prieto-Mahaney, O.O.; Li, D.; Abe, R. What is Degussa (Evonik) P25? Crystalline composition analysis, reconstruction from isolated pure particles and photocatalytic activity test. *J. Photochem. Photobiol. A.* **2010**, *216*, 179–182, https://doi.org/10.1016/j.jphotochem.2010.07.024.
38. El-Mekkawi, D.; Galal, H.R. Removal of a synthetic dye "Direct Fast Blue B2RL" via adsorption and photocatalytic degradation using low cost rutile and Degussa P25 titanium dioxide. *J. Hydro-Environ. Res.* **2013**, *7*, 219–226, https://doi.org/10.1016/j.jher.2013.02.003.
39. Najdanovic, S.; Mitrovic, J.; Zarubica, A.; A. Bojic, The effectof operational parameters on decolourisation of textile and comparison efficiencies of the UV/H_2O_2, Fenton and photo-Fenton processes: A Review. *FACTA Universitatis, Physics, Chemistry and Tecnology* **2017**, *15*, 23-34, https://doi.org/10.2298/FUPCT1701023N.
40. Muruganandham, M.; Swaminathan, M. Solar driven decolourisation ofreactive yellow 14 by advanced oxidation processes in heterogeneous and homogeneous media. *Dyes Pigm.* **2007**, *72*, 137–143, https://doi.org/10.1016/j.dyepig.2005.08.009.
41. Chu, W.; Choy, W.K.; So, T.Y. The effect of solution pH and peroxide in theTiO_2-induced photocatalysis of chlorinated aniline. *J. Hazard. Mater.* **2007**, *141*, 86–91, https://doi.org/10.1016/j.jhazmat.2006.06.093.
42. Ho, Y.S.; Mckay, G. The kinetic of sorption of basic dyes from aqueous solution by sphagnum Moss peat. *J. Chem. Eng.* **1998**, *76*, 822-827, https://doi.org/10.1002/cjce.5450760419.
43. Guettaı, N.; Amar, H.A. Photocatalytic oxidation of methyl orange in presence of titanium dioxide in aqueous suspension. Part II: kinetics study. *Desalination* **2005**, *185*, 439–448, https://doi.org/10.1016/j.desal.2005.04.049.

 doi:10.20944/preprints202103.0123.v1

44. Author 1, A.B.; Author 2, C.D. Title of the article. *Abbreviated Journal Name* **Year**, *Volume*, page range.
45. Author 1, A.; Author 2, B. Title of the chapter. In *Book Title*, 2nd ed.; Editor 1, A., Editor 2, B., Eds.; Publisher: Publisher Location, Country, 2007; Volume 3, pp. 154–196.
46. Author 1, A.; Author 2, B. *Book Title*, 3rd ed.; Publisher: Publisher Location, Country, 2008; pp. 154–196.
47. Author 1, A.B. (University, City, State, Country); Author 2, C. (Institute, City, State, Country). Personal communication, 2012.
48. Author 1, A.B.; Author 2, C.D.; Author 3, E.F. Title of Presentation. In Title of the Collected Work (if available), Proceedings of the Name of the Conference, Location of Conference, Country, Date of Conference; Editor 1, Editor 2, Eds. (if available); Publisher: City, Country, Year (if available); Abstract Number (optional), Pagination (optional).
49. Author 1, A.B. Title of Thesis. Level of Thesis, Degree-Granting University, Location of University, Date of Completion.
50. Title of Site. Available online: URL (accessed on Day Month Year).